

A COMPARATIVE STUDY OF SERIAL AND PARALLEL FLOWS OF THE SWEEPING GAS IN TUBULAR MEMBRANE REACTOR IN THE PRESENCE OF CATALYST DEACTIVATION FOR CATALYTIC NAPHTHA REFORMING PROCESS

H. Nouryzadeh, D. Iranshahi

Chemical Engineering Department, Amirkabir University of Technology, Tehran 15875, Iran

Received April 14, 2014, Accepted June 30, 2014

Abstract

In this study, two modes of the sweeping gas flow in a tubular membrane reactor (TMR) are taken into consideration for catalytic naphtha reforming process. The performance of the parallel configuration is compared with the serial one. The effects of the membrane thickness and hydrogen mole fraction in the sweeping gas are investigated on the required compressors' pressures and hydrogen and aromatic yields. Set of coupled PDEs are solved by the orthogonal collocation method. Results show that the parallel configuration performs better than the serial one from operating and heat transfer viewpoints. TMR with the parallel flow of the sweeping gas is superior to the serial one owing to the independent operation of reactors. Since variables in the parallel flow are easier to design and control than the serial ones, a parallel flow is recommended for naphtha reforming process.

Keywords: Catalytic naphtha reforming; Tubular membrane reactor; Parallel and Series sweeping gas flow modes; Catalyst deactivation.

1. Introduction

Catalytic naphtha reforming plays a major role in the total benefits of all refinery complexes. A vast variety of research areas has been focused on this process to improve its operational conditions and to achieve more products yield. Benitez *et al.* [1], Mazzieri *et al.* [2], Viswanadham *et al.* [3], Boutzeloit *et al.* [4], Carvalho *et al.* [5] and Beltramini *et al.* [6] investigated the effect of various metal bases on the catalyst activity and the reforming yield. Attempts have been made to achieve higher efficiency of the process, better use of the available feedstocks and the processing of alternative raw materials [1]. Ren *et al.* [7] investigated a series of naphtha reforming catalysts from different stages of coking and the regeneration processes by NMR and chemical engineering methods. Many kinetic studies have been conducted on the complex naphtha chain reactions in order to predict the reforming compositions more accurately. Smith [8] was the pioneer of this field of studies. Ramage *et al.* [9-10] developed a detailed kinetic model based on studies of an industrial pilot plant reactor. Krane *et al.* [11] recognized the presence of various carbon numbers for reforming reactions. Other studies have been done by Weifeng *et al.* [12], Kmak [13], Boyas and Froment [14], Stijepovic *et al.* [15] and Marin *et al.* [16]. Iranshahi *et al.* [17] studied the catalytic naphtha reforming in the radial flow spherical reactors to decrease the pressure drop and to increase the aromatic production. Rahimpour [18], Kolesnikov *et al.* [19] investigated the catalytic naphtha reforming in fluidized bed reactors. Min *et al.* [20] modeled a four stages catalytic reforming unit with a radial flow pattern. Optimization of operating conditions in naphtha reforming process has been performed to increase the aromatic yield and annual profits [21-26].

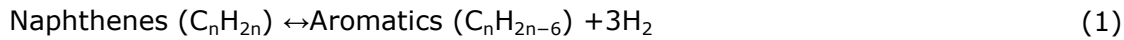
The objective of this study is to compare the effect of applying the parallel flow with the serial flow of the sweeping gas on the TMR performance in naphtha reforming process. In order to model the TMR configuration, a heterogeneous model is considered. A catalyst deactivation model is applied to investigate the effect of catalyst deactivation on the performance of TMR. Since the walls of the tubes in TMR are coated by the Pd-Ag membrane layer, the effect of hydrogen permeation is taken into consideration in mass and energy balances. A set of coupled

PDEs are solved by the orthogonal collocation method. The modeling results are compared with the plant data of the conventional tubular reactor (CTR). This study demonstrates that TMR with the parallel flow of the sweeping gas performs better than the serial one in some cases as will be described further.

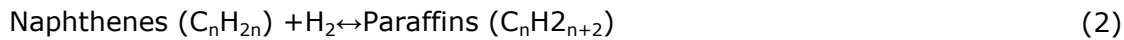
2. Reactions and Kinetic scheme

A kinetic model is considered based on the Smith's model [8]. Smith assumed some pseudo-components to simplify the feedstock of catalytic naphtha reforming. Thus, four dominant idealized reactions can be taken into consideration as follows:

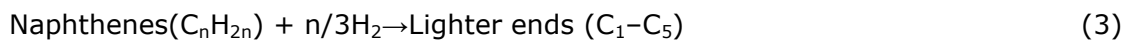
- Dehydrogenation of naphthenes to aromatics.



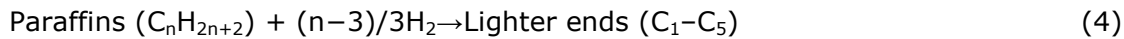
- Dehydrocyclization of paraffins to naphthenes.



- Hydrocracking of naphthenes to lower hydrocarbons.



- Hydrocracking of paraffins to lower hydrocarbons.



The naphtha reforming reactions are limited by equilibrium; in order to achieve high aromatic production, they should be carried out at a high temperature. The rate equations for these reactions are as follows:

$$r_1 = \left(\frac{k_{f1}}{K_{e1}}\right)(k_{e1}p_n - p_a p_h^3) \quad (5)$$

$$r_2 = \left(\frac{k_{f2}}{K_{e2}}\right)(k_{e2}p_n p_h - p_p) \quad (6)$$

$$r_3 = \left(\frac{k_{f3}}{p_t}\right)p_n \quad (7)$$

$$r_4 = \left(\frac{k_{f4}}{p_t}\right)p_p \quad (8)$$

where k_{f_i} and K_{e_i} are forward rate constant and equilibrium constant, respectively. The equations of these constants for the reactions are reported by Rase [27].

$$k_{f1} = 9.87 \exp\left(23.21 - \frac{E_1}{1.8T}\right)a \quad (9)$$

$$k_{f2} = 9.87 \exp\left(35.98 - \frac{E_2}{1.8T}\right)a \quad (10)$$

$$k_{f3} = k_{f4} = \exp\left(42.97 - \frac{E_3}{1.8T}\right)a \quad (11)$$

$$K_{e1} = 1.04 \times 10^{-3} \exp\left(46.15 - \frac{46045}{1.8T}\right) \quad (12)$$

$$K_{e2} = 9.87 \exp\left(-7.12 + \frac{8000}{1.8T}\right) \quad (13)$$

where a is the catalyst activity and E is the activation energy of related reaction. The activation energies depend on the catalyst which is used. The activation energies are derived using the previous work by Khosravanipour and Rahimpour [28]. The activation energies are as follows: $E_1=36350$; $E_2=58550$; $E_3=63800$.

3. Process Description

3.1. Conventional process (CTR)

A simplified process flow diagram for CTR is depicted in Fig.1. The naphtha feed is mixed with the recycled gas containing 60-90% (by mole) hydrogen and preheated before entering the 1st reactor. Reactors are packed with catalysts and the chemical reactions take place on catalysts' surfaces. Since naphtha reforming is an endothermic process, the outlet stream must be preheated before entering the following reactor by inter-stage heaters. In order to stabilize the liquid and separate the gaseous product, the effluent from the 3rd reactor is cooled and directed into the separators. The liquid product is called reformat which mainly consists of aromatics (60–70 mass% of naphtha feed) and saturates in the C₅–C₉ carbon range. The equilibrium conversion increases by increasing temperature owing to the endothermic reaction. The improvement in the octane number of reformat is achieved by lowering space velocity, raising the inlet temperature of the reactor at a constant pressure and shifting the reaction to the aromatic production by hydrogen removal from the reaction side (e.g. by using the membrane technology). The main reactions in the first reactor are dehydrogenation and isomerization, in the second reactor are dehydrogenation, isomerization, cracking and dehydrocyclization and in the third one are cracking and dehydrocyclization [28]. The operating conditions of CTR are described in Table1.

Table 1 Specifications of conventional naphtha reactor, feed, product and catalyst of plant for fresh catalyst.

parameter	Numerical Value	unit
Naphtha feed stock	30.41×10^3	Kg/hr
Reformat	24.66×10^3	Kg/hr
H ₂ /HC mole ratio	4.74	–
LHSV	1.25	hr ⁻¹
Mole percent of hydrogen in recycle	69.5	–
Diameter and length of 1 st reactor	1.25, 6.29	m
Diameter and length of 2 nd reactor	1.67, 7.13	m
Diameter and length of 3 rd reactor	1.98, 7.89	m
Distillation fraction of naphtha feed and reformat		
TBP	Naphtha feed (°C)	Reformat (°C)
IBP	106	44
10%	113	73
30%	119	105
50%	125	123
70%	133	136
90%	144	153
FBP	173	181
Typical properties of catalyst		
d _p	1.2	mm
Pt	0.3	wt%
Re	0.3	wt%
s _a	220	m ² /g
ρ _B	0.3	Kg/l
ε	0.36	–

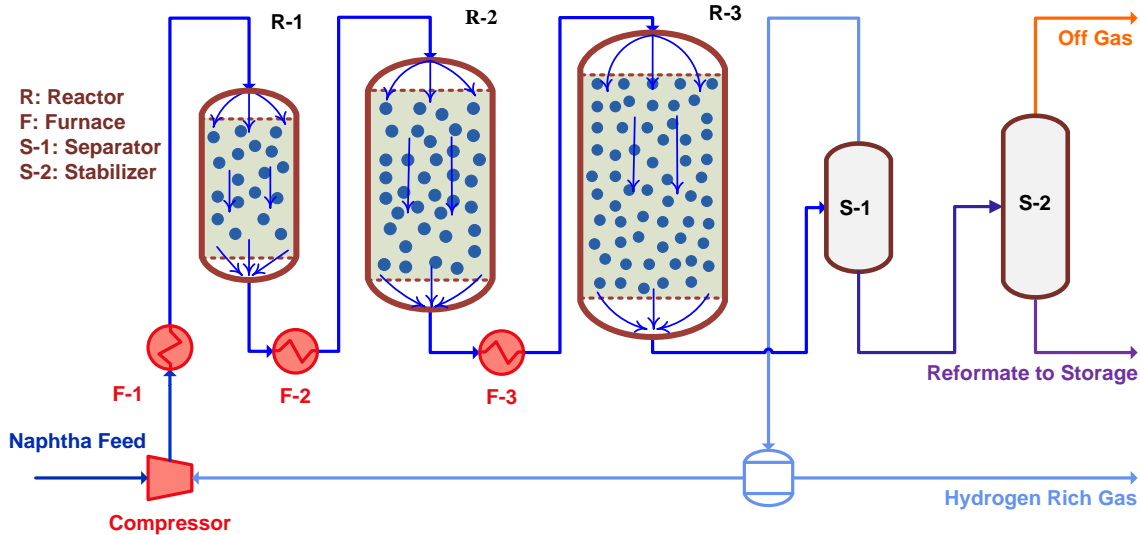


Figure.1 A simple process flow diagram for conventional catalytic naphtha reforming (CTR)

3.2. Tubular Membrane Reactor Setup

3.2.1 Tubular Membrane reactor with the serial flow of the sweeping gas

Fig.2 illustrates the process flow diagram for TMR in which the sweeping gas lines are serial. In a serial mode, the sweeping gas enters the shell side of the first reactor and it is enriched by hydrogen as proceeding along the reactor. Subsequently, the outlet stream from the shell side enters the next reactor. As a result, the performance of the reactors in the serial configuration is dependent to each other. The potential difference, hydrogen permeation driving force, decreases along each reactor. According to the Sievert's law, the driving force (hydrogen permeation) is proportional to the hydrogen partial pressure difference between shell and tube sides of each reactor. The specification of this membrane reactor extensively described in the previous work [28].

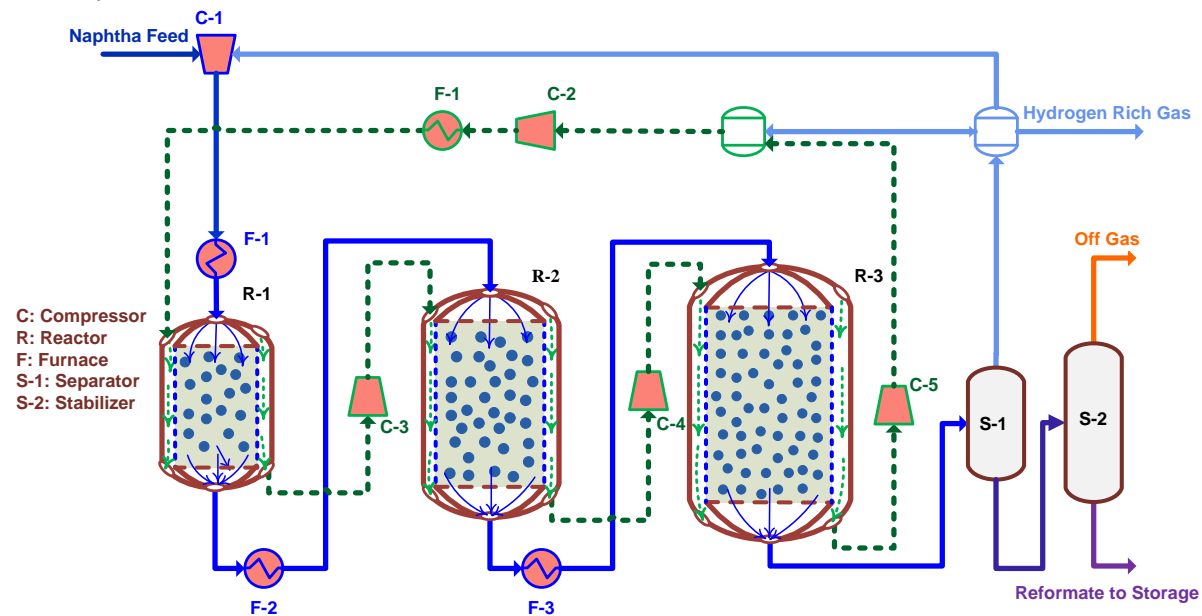


Figure.2 Schematic diagram of tubular membrane reactor (TMR) with the serial flow of the sweeping gas.

3.2.2 Tubular Membrane reactor with the parallel flow of the sweeping gas

The scheme of the TMR with parallel sweeping gas lines is depicted in Fig.3. The basic idea of a "parallel" configuration is to connect all reactors with lower hydrogen partial pressure.

In a word, lower hydrogen partial pressure is equivalent to higher hydrogen permeation rate. This leads to the selection of a thicker and a durable membrane. The only difference between the parallel configuration and the serial one is the sweeping gas distribution lines. In the parallel flow, the potential is the same along each reactor unlike the serial flow where it decreases as the sweeping gas is flowing along reactors. As seen, branches provide separate paths for the sweeping gas flows. Since the main current of the sweeping gas is divided into separate pathways, a break in one or more of those pathways does not interrupt the flow in the other paths. Consequently, reactors operate independently. The total amount of hydrogen is equal to the sum of the currents in each branch. In the parallel flow, the sweeping gas molar flow rate in each branch is one third of the total amount. Thus, the inlet molar flow rate of the sweeping gas equals 500 kmol/hr. Moreover, the inlet temperature of the sweeping gas is the same for all reactors. The specification of the sweeping gas and the operating conditions of TMRs are illustrated in Table 2.

Table 2 Specifications for sweep gas and permeation side in both series and parallel configurations.

	Inlet sweep gas temperature (K)	Inlet sweep gas pressure (kPa)	Inlet sweep gas flow (kmole/hr)	Inlet sweep gas composition (H ₂ %)
Series sweep gas flow				
1 st reactor	777	1650	1500	69.5
2 nd reactor	–	2120	–	–
3 rd reactor	–	2145	–	–
Parallel Sweep gas flow				
1 st reactor	777	1610	500	69.5
2 nd reactor	777	2145	500	69.5
3 rd reactor	777	2172	500	69.5
Additional information				
Membrane thickness (μm)	10		Hydraulic diameter (m)	0.1

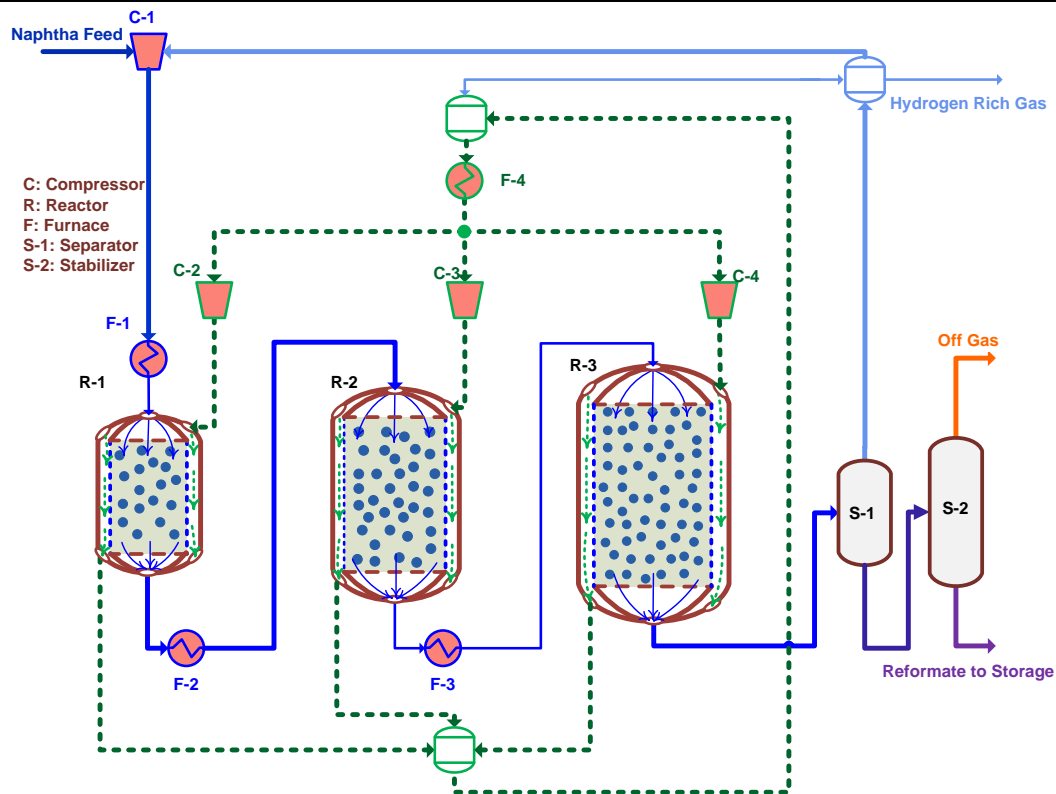


Figure 3 Schematic diagram of tubular membrane reactor (TMR) with the parallel flow of the sweeping gas.

4. Reactor model

The main structure of the model is initiated by the previous work which carried out by Khosravanipour and Rahimpour [28]. The new approach given by this study relies on some modifications which are considered to improve the model capability. The mass and energy balance equations (for both shell and tube sides) together with the pressure drop correlations [29] and a catalyst deactivation model [30] are presented in Table 3. The notations are presented in the nomenclature in Appendix C.

Table 3 Mass & Energy balances for tubular membrane reactor.

Fluid phase (Tube side)	
$D_{ej} \left(\frac{\partial^2 C_j}{\partial z^2} \right) - \frac{\partial(u_z C_j)}{\partial z} + \rho_B a \sum_{i=1}^m v_{ij} r_i$	(10)
$-\frac{4J_{H_2}}{D} = \varepsilon \frac{\partial C_j}{\partial t} \quad j=1,2,\dots,n \quad i=1,2,\dots,m$	
$k_{eff} \left(\frac{\partial^2 T_{Tube}}{\partial z^2} \right) - \frac{\partial}{\partial z} (\rho u_z C_p (T_{Tube} - T_{ref})) + \left(\frac{4J_{H_2}}{D} C_p (T_{Shell} - T_{Tube}) \right)$	(11)
$+ \left(\frac{4U}{D} (T_{Shell} - T_{tube}) \right) + \rho_B a \sum_{i=1}^m \Delta H_i r_i = \varepsilon \frac{\partial}{\partial t} (\rho C_p (T_{Tube} - T_{ref}))$	
Solid phase (Tube side)	
$k_{c_j} s_a (C_j - C_j^s) + \sum_i v_{ij} r_i = 0$	(12)
$hs_a (T - T^s) + \sum_i v_{ij} (-\Delta H_i) r_i = 0$	(13)
Fluid phase (Shell side)	
$D_{ej} \left(\frac{\partial^2 C_j}{\partial z^2} \right) - \frac{\partial(u_z C_j)}{\partial z} + \frac{4J_{H_2}}{D} = \varepsilon \frac{\partial C_j}{\partial t} \quad j=1,2,\dots,n \quad i=1,2,\dots,m$	(14)
$k_{eff} \left(\frac{\partial^2 T_{Shell}}{\partial z^2} \right) - \frac{\partial}{\partial z} (\rho u_z C_p (T_{Shell} - T_{ref})) - \left(\frac{4J_{H_2}}{D} C_p (T_{Shell} - T_{Tube}) \right)$	(15)
$- \left(\frac{4U}{D} (T_{Shell} - T_{tube}) \right) = \varepsilon \frac{\partial}{\partial t} (\rho C_p (T_{Shell} - T_{ref}))$	
Hydrogen permeation rate	
$J_{H_2} = \frac{Q_0 \exp\left(-\frac{E_{H_2}}{RT}\right)}{\delta_{H_2}} \left(\sqrt{P_{H_2}^{tube}} - \sqrt{P_{H_2}^{Tube}} \right) [Abo-Ghander et al.]$	(16)
$Q_0 = 1.65 \times 10^{-5} \text{ molm}^{-1} \text{ s}^{-1} \text{ pa}^{-\frac{1}{2}}, E_{H_2} = 15.7 \text{ kJmol}^{-1}$	
Boundary & initial conditions	
$z=0: C_j = C_{j0}, T = T_0$	(17)
$z=L: \frac{\partial C_j}{\partial z} = 0, \frac{\partial T}{\partial z} = 0$	(18)
$t=0; C_j = C_j^{ss}, T = T^{ss}, T_s = T_s^{ss}; a=1;$	(19)
Ergun equation (Pressure drop)	
$\frac{dP}{dz} = \frac{150\mu (1-\varepsilon)^2}{\phi_s^2 d_p^2} \frac{Q}{\varepsilon^3 A_c} + \frac{1.75\rho (1-\varepsilon)}{\phi_s d_p} \frac{Q^2}{\varepsilon^3 A_c^2}$	(20)

Catalyst deactivation

$$\frac{da}{dt} = -K_d \exp\left(-\frac{E_d}{R} \left(\frac{1}{T} - \frac{1}{T_R}\right)\right) a^7 \quad (21)$$

$$T_R = 770K, E_d = 1.642 \times 10^5 \text{ jmol}^{-1}, K_d = 5.926 \times 10^{-5} \text{ h}^{-1}$$

The following assumptions are made for both shell and tube sides in the mathematical modeling of TMR:

- (i) One dimensional plug flow is assumed.
- (ii) Radial dispersions of heat and mass are neglected.
- (iii) The gas is supposed to be ideal.

A set of auxiliary correlations which are used in the modeling are presented in Appendix B.

5. Numerical Solution

A set of coupled PDEs including energy and mass balances as well as ODE and algebraic equations of the system are solved by the orthogonal collocation method (Appendix A). The deactivation model is an ODE. The auxiliary correlations, kinetics and thermodynamics of the reaction systems constitute a set of algebraic equations. More details concerning this subject was presented by Iranshahi *et al.* [17].

6. Model validation

6.1. Unsteady state model validation

Model validation is carried out by a comparison between the modeling results of TMR and the historical process data. The predicted results of production rate, the corresponding observed data and the residual errors are presented in Table 4. As seen, the model performs well under industrial conditions and there exists a good agreement between the daily-observed plant data and the modeling results. Boiling point ranges are determined by Distillation Petro Test D86 [31].

Table 4 Unsteady state model validation.

Time (day)	Naphta feed (ton/hr)	Plant (kmol/hr)	Tubular (kmol/hr)	Devi % (Tubular- Plant)
0	30.41	225.90	221.7819	-1.8230
34	30.41	224.25	222.7137	-0.6851
62	31.00	229.65	228.1372	-0.6588
97	30.78	229.65	226.9795	-1.1629
125	31.22	229.65	231.0067	0.5908
160	31.22	229.65	231.4815	0.7975
188	28.55	211.60	210.0259	-0.7439
223	30.33	222.75	224.9212	0.9747
243	31.22	233.05	232.3911	-0.2827
298	30.67	228.65	228.3803	-0.1179
321	30.76	227.64	229.2991	0.7288
398	42.35	317.30	324.8447	2.3778
425	42.32	317.94	324.7715	2.1487
461	42.32	317.94	324.9876	2.2166
490	42.32	317.94	325.1511	2.2681
524	42.32	313.09	325.3321	3.9101
567	42.54	317.94	327.3489	2.9593
610	42.54	313.90	327.5484	4.3480
717	37.86	286.15	289.6324	1.2170
771	38.51	282.10	295.1652	4.6314

6.2. Steady state model validation

In order to verify the efficiency of the steady state model, the modeling results are compared with observed plant data of CTR. Table 5 illustrates the plant data and the predicted mole fractions of components in the output of the system. Model results show a good agreement

with the plant data. Analyses of components (paraffin, naphthene and aromatic) are performed by PONA Test in Stan Hop Seta apparatus. The aromatic is tested especially by ASTM 2159 equivalent to UOP 273 method [31].

Table 5 Comparison between model prediction and plant data for fresh catalyst

Reactor number	Inlet temperature (K)	Inlet pressure (kPa)	Catalyst distribution (wt %)	Input feedstock (mole %)			
1	777	3703	20	Paraffin	49.3		
2	777	3537	30	Naphthene	36		
3	775	3401	50	Aromatic	14.7		
Reactor number	Outlet temperature (K)			Aromatic in reformat (mole %)			
	Plant	CTR		plant	CTR	Series	Parallel
1	722	732.1		-	34.95	36.32	35.69
2	753	757.5		-	47.44	48.59	48.50
3	770	772.5		57.7	56.82	58.09	59.30

7. Results and Discussion

The H_2/HC versus the dimensionless mass of catalyst for CTR and TMRs is depicted in Fig.4. This ratio is one of the restricted parameters in the controlling unit of the naphtha reforming process. It is adjusted according to the inlet amount of feed to the first reactor. In industry, it is recommended to maintain the H_2/HC in the range of 4-6 [31]. If the H_2/HC becomes lower than 4, the catalysts will be subjected to coking and a rapid deactivation. It imposes a huge burden on catalysts and jeopardizes the catalyst life. On the other hand, high ratios decrease the aromatic production because the first equilibrium reaction shifts to the reactants side which leads to aromatic consumptions. In TMRs, the membrane layer enables to maintain H_2/HC at approximately the inlet amount of 4.73 by the help of the permeation pressures. Unlike membrane reactors where it maintains approximately constant, H_2/HC increases gradually in CTR. The related permeation pressures are mentioned in Table 2.

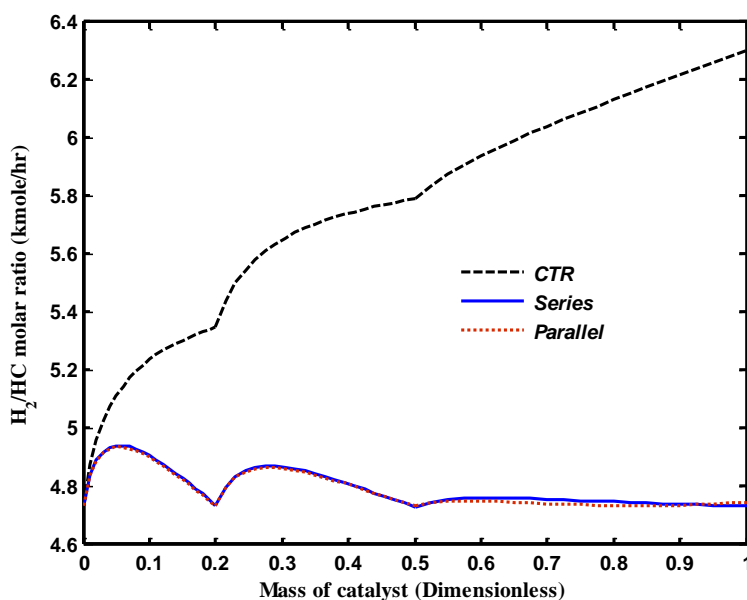


Figure 4 The H_2/HC molar ratio along CTR and TMRs.

The temperature profile of TMR with serial flow of the sweeping gas (for shell and tube sides) along three reactors is depicted in Fig.5 (a). The tube side temperature decreases abruptly in the 1st reactor due to the endothermic reaction in the tube side. Also, the sweeping gas temperature decreases due to the convective heat transfer with the tube side (reaction side).

In the 2nd reactor, heat transfers from the tube side to the shell side which causes a maximum in the shell side temperature. Nevertheless, this is not exactly what we look for. The temperature in the shell side decreases in the rest of the 2nd reactor length. As Fig.5 (a) shows, the heat transfer always takes place from the tube side to the shell side of the 3rd reactor. This is improper for the 2nd and the 3rd reactors in the serial flow. The same attitude as the serial configuration is considered for analyzing and understanding the thermal behavior of the parallel flow (Fig.5 (b)). The inlet temperature of the sweeping gas to the three reactors is kept at 777 K in the parallel flow. As a result, the sweeping gas temperature is always more than the reaction side temperature and heat transfers from the shell side to the tube side.

In industry, reactors are insulated in order to prevent thermal loss. In the parallel flow, the sweeping gas acts as an external protect (secondary insulation) against the events happening in the reaction side owing to its higher temperature than the serial one. Moreover, if the circumstances influence the reaction side, changes will affect the sweeping gas more than the reaction side. Thus, the reaction side is impressed less than the sweeping gas by the variations. It can be considered as one of the advantages of the parallel flow in comparison with the serial one.

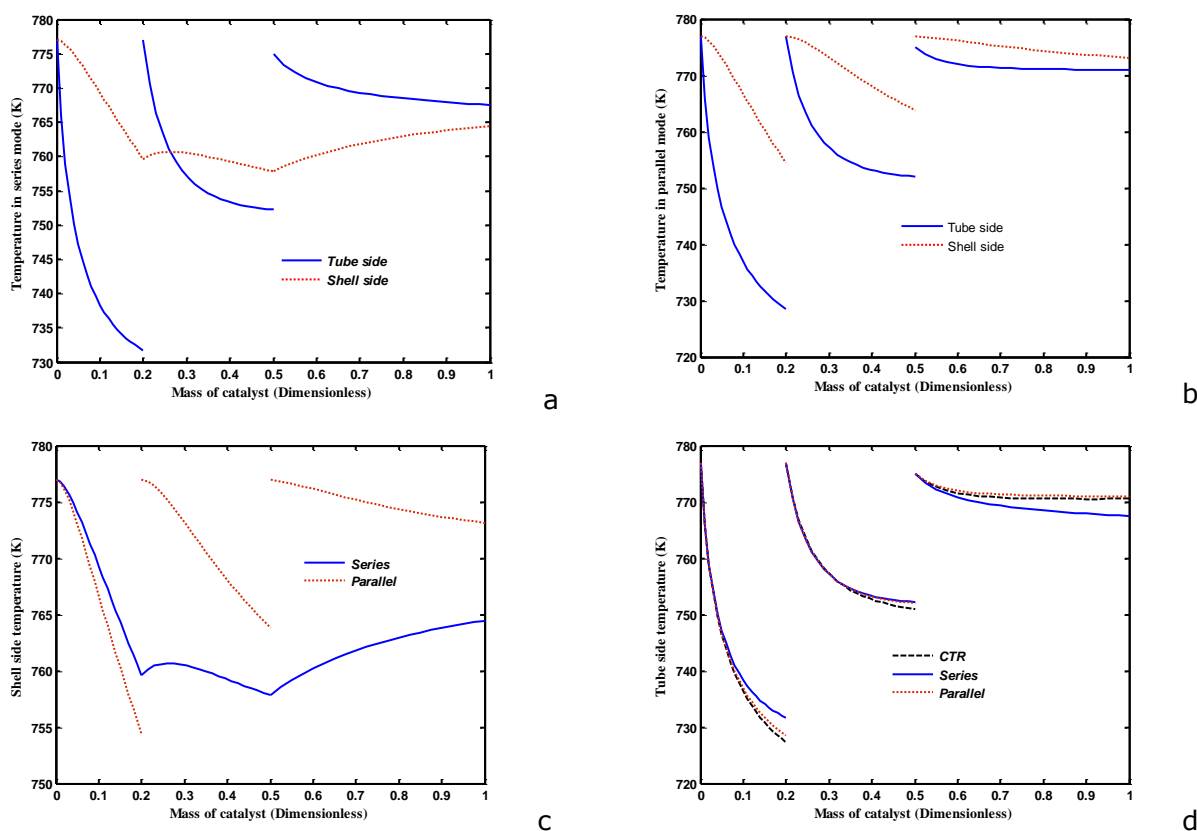


Figure.5 Temperature profile of (a) shell and tube sides in a serial flow (b) shell and tube sides in a parallel flow and (c) shell side in serial and parallel flows of TMR (d) tube side along CTR and TMRs.

The shell side temperature along the three reactors for serial and parallel flows is depicted in Fig.5(c). The shell side temperature in the parallel flow is higher than the one in the serial flow except for the first reactor. In the parallel flow, inlet temperatures of three reactors are the same. The shell side temperature falls abruptly in the first reactor of the parallel configuration in comparison with the one of the serial configuration due to lower feed flow rate in the parallel flow.

Fig.5 (d) compares the tube side temperature along CTR and TMR (for serial and parallel flows). Owing to providing a heat source by a sweeping gas in the shell side, the temperatures will be higher in the tube side of TMRs in comparison with CTR. This is in favor of the endothermic reactions in naphtha reforming. The naphtha molar flow rate in the serial flow is

higher than the parallel one. According to the relationship between the Nusselt number and the Reynolds number, the velocity and the heat transfer coefficient of the serial flow is higher than the ones in the parallel flow. Thus, the temperature drop in the serial flow is less than the parallel flow. The trend of the tube side temperature in the 2nd reactor is similar to the one in the 1st reactor. The order of temperature profiles for the 3rd reactor is obviously illustrated in Fig.5 (a)-(b). In the 3rd reactor, the highest temperature drop occurs for the serial flow because the sweeping gas temperature is less than the reaction side temperature. Nevertheless, the temperature drop in the parallel flow is the least.

Fig.6 illustrates hydrogen mole fraction in the shell side of TMRs. In the serial flow of the sweeping gas, hydrogen with a specific mole fraction leaves the 1st reactor and enters serially the 2nd reactor. The sweeping gas is enriched by hydrogen as it is proceeding along the reactors. Therefore, the hydrogen mole fraction increases continuously along the three reactors for the serial flow of the sweeping gas. As a result, the driving force for hydrogen permeation between shell and tube sides decreases in the serial flow and hydrogen mole fraction tends to be constant in the 3rd reactor. On the other hand, the inlet mole fraction of hydrogen equals 0.695 in the parallel configuration. In TMR configuration with the parallel flow of the sweeping gas, hydrogen permeates through a membrane layer from the reaction side to the shell side in three reactors thus, its mole fraction increases in the shell side of each reactor. Unlike the serial flow, the mole fraction of the sweeping gas is independent of each other, thus the reactors operate independently for the parallel flow of the sweeping gas. If there is a technical defect in the sweeping gas lines of the serial configuration, the sweeping gas lines should be closed in order to hinder its effect from the subsequent reactors. However, the reactors perform well if the same circumstance exists in the parallel configuration. This figure also shows a significant difference in the hydrogen mole fraction in the parallel flow in comparison with the one in the serial flow. Due to higher hydrogen molar flow rate in the serial flow than the parallel one (three times higher than the parallel), its mole fraction does not change considerably in the 1st reactor. The hydrogen mole fractions are 0.758 and 0.757 in the parallel and series flow, respectively.

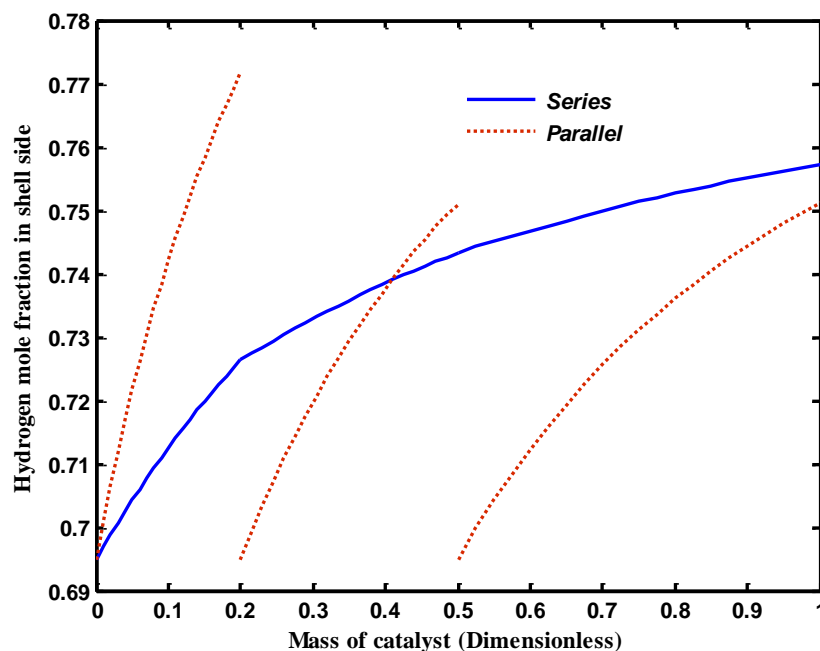


Figure.6 Hydrogen mole fraction in the shell side along TMRs.

Fig.7 (a)-(b) illustrate the reactant consumption rates along CTR and TMRs. Paraffin molar flow rate for CTR and TMRs is depicted in Fig.7 (a). The paraffin consumption rate in the 1st and the 2nd reactors of TMR configuration is similar for the parallel and serial flows. The effectiveness of membrane is evidently demonstrated by comparing the paraffin molar flow rate in CTR and TMRs. According to the Le Chatelier's principle, the second equilibrium reaction shifts

back to the reactant side due to the hydrogen removal from the reaction side. As a result, more paraffin is consumed in TMRs in comparison with CTR. The difference between the paraffin consumption rate in serial and parallel flows becomes more evident in the 3rd reactor. It can be justified by temperature profiles of the 3rd reactor (see Fig.5 (d)). The naphthene consumption rate is equal in the beginning lengths of the first reactor of CTR and TMRs. Owing to high reaction rates, the effect of membrane in shifting the reactions can be ignored (see Fig.7 (b) for the 1st reactor). The flow rate arrangement at the outlet of the first reactor implies that how the reaction temperature can affect the naphthene consumption.

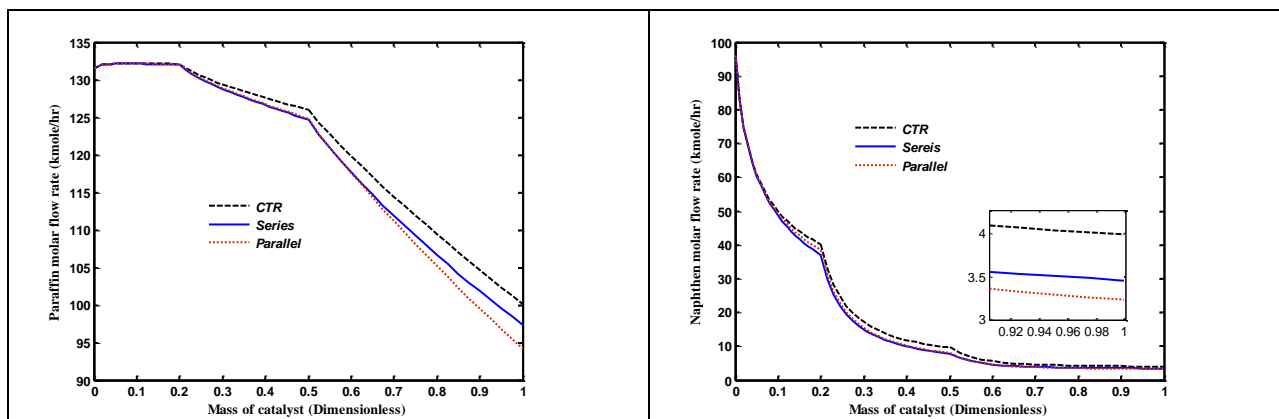


Figure.7 (a) Paraffin molar flow rate and (b) Naphtha molar flow rate along CTR and TMRs.

Fig.8 (a) demonstrates the capability of using membrane to increase the aromatic production in refineries. The aromatic production for the serial flow is more considerable than the parallel one in the 1st and the 2nd reactors. In the 3rd reactor, the aromatic production rate for the parallel flow is higher than the serial flow due to higher temperature of the 3rd reactor. These occurrences are justified by the reaction side temperatures (see Fig.5 (d)). Considering the small graph in Fig.8 (a) shows that the increase in the aromatic yield in the parallel flow is approximately 1kmol/hr more than the one in the serial flow which becomes a considerable amount per year. The light ends molar flow rate is presented in Fig.8 (b).

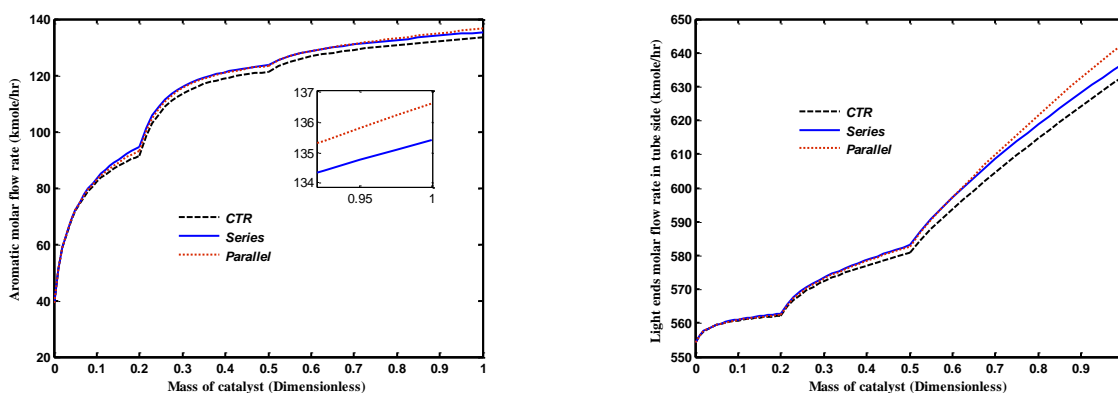


Figure.8 (a) Aromatic molar flow rate and (b) Light ends molar flow rate along CTR and TMRs.

The total hydrogen production rate has the same trend as the aromatic production rate shown in Fig.9 (a). It is worth mentioning that the total hydrogen is produced just because of the reaction (no recycle added). The hydrogen molar flow rate increases in the tube side of CTR (Fig.9 (b)). However, it decreases in the tube side of TMRs owing to the hydrogen permeation through the membrane layer to the shell side. A peak in the hydrogen molar flow profile of TMR shows that the hydrogen production rate is higher than the hydrogen permeation rate through the membrane layer in the 1st and the 2nd reactors. Furthermore, no difference is observed between the hydrogen molar flow rates in TMRs due to a high hydrogen production rate.

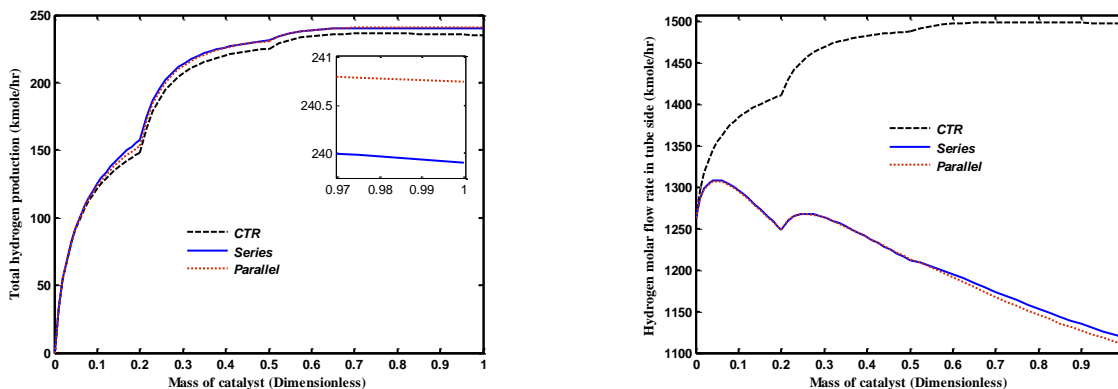


Figure.9 (a) The total hydrogen production in CTR and TMRs (hydrogen in the permeation side plus the hydrogen content of tube side) and (b) the hydrogen molar flow rate in the tube side along the reactor length for CTR and TMRs.

As previously mentioned, some modifications are considered to improve the modeling results. Thus, the total molar flow rate, molecular weight, heat capacity, viscosity, density and, etc. are considered to be variable. Fig.10 (a)-(b) illustrate how the total molar flow rate and molecular weight change along the reactors. The average molecular weight of the gas phase increases in TMRs due to the hydrogen removal from the reaction side. The minimum points in the graph of the molecular weight (Fig.10 (b)) are proportional to the maximums in Fig.10 (a).

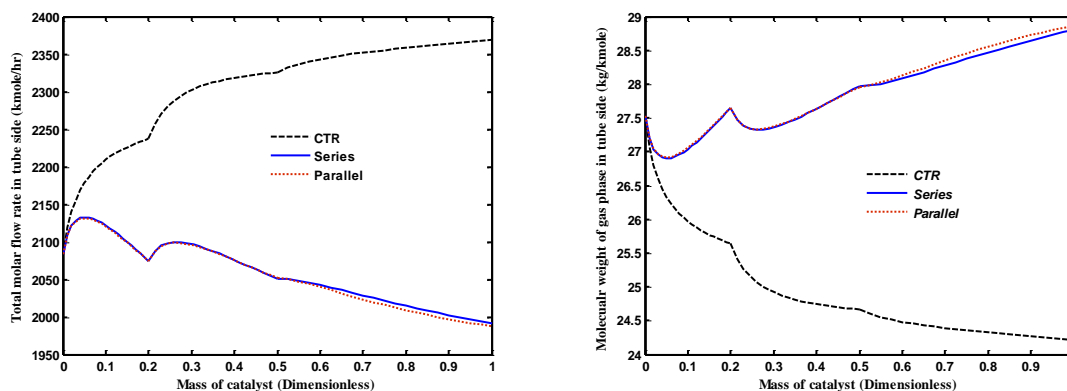


Figure.10 (a) Total molar flow rate in the tube side of CTR and TMRs (b) the average molecular weight of the gas phase in the tube side of CTR and TMRs versus the mass of catalyst.

The pressure profile along CTR and TMRs is depicted in Fig.11. The pressure drop for both flows in TMRs is lower than CTR. Since hydrogen permeates through the membrane layer to the shell side, the total molar flow rate decreases in the reaction side. Accordingly, the velocity and related viscous loss (pressure drop) are lower than the one in CTR owing to lower molar flow rate.

The effect of hydrogen mole fraction in the sweeping gas on the products yield and the required pressures of permeation side (to have a desired H_2/HC) are investigated in the following figures.

Firstly, its effect on the required pressures of the sweeping gas in three reactors is investigated and two case studies (I, II) are taken into consideration in this regard. If the hydrogen mole fraction decreases, the compressor pressure should be increased to maintain H_2/HC above 4.73. The effect of hydrogen mole fraction in the sweeping gas on the required pressure of the sweeping gas is investigated for two case studies in Fig. 12(a)-(c). In case I ($\delta_1=\delta_2=\delta_3=10\mu m$), by increasing the hydrogen mole fraction in the sweeping gas, the required pressure of the sweeping gas decreases in three reactors. As membranes' thicknesses increase as case II ($\delta_1=30\mu m$, $\delta_2=50\mu m$, $\delta_3=70\mu m$) the required pressures of

the sweeping gas do not change considerably for all three reactors. Thus, thicker membranes are excellent choices against the increasing pressure in the permeation sides.

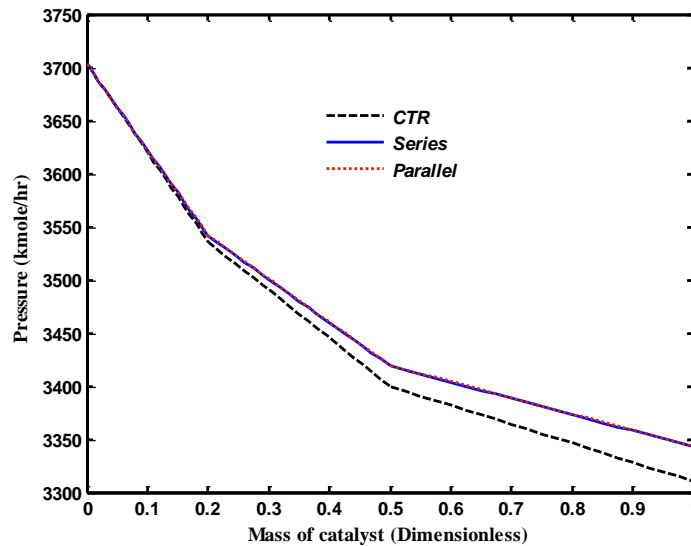


Figure.11 Pressure profile along CTR and TMRs.

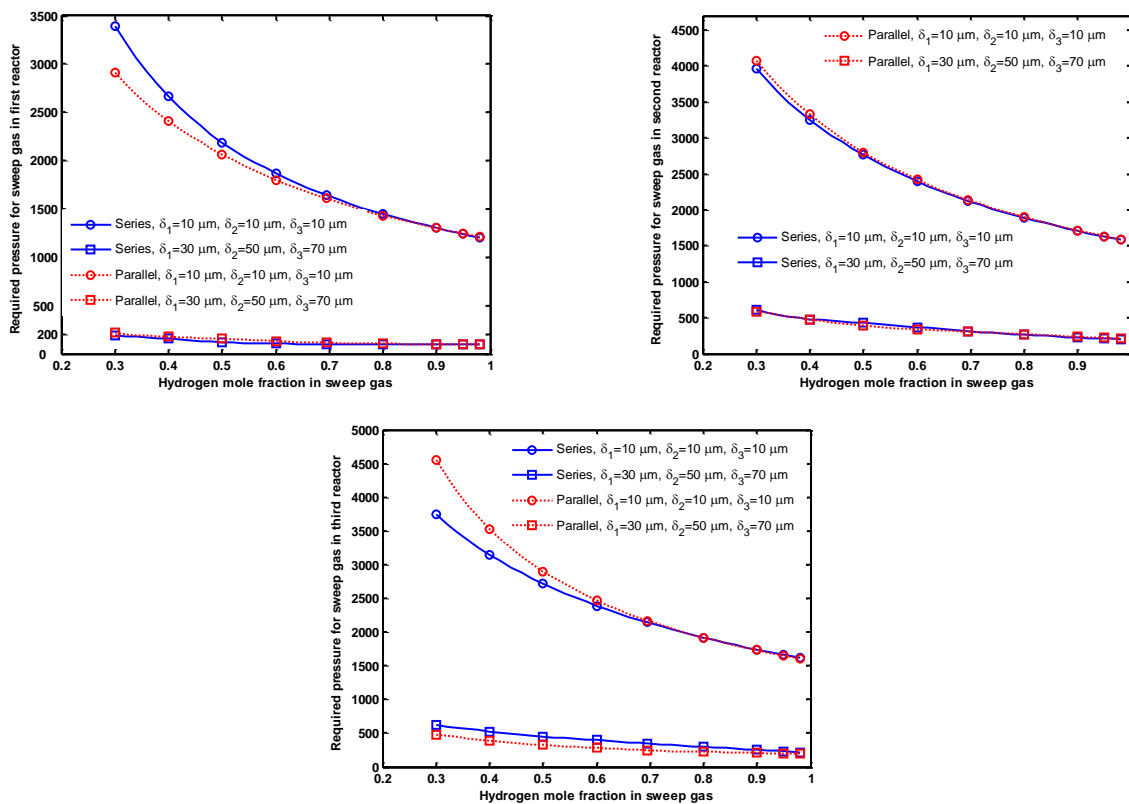


Figure.12 Required pressure for the sweeping gas in (a) the first reactor (b) the second reactor (c) the third reactor versus the hydrogen mole fraction in the sweeping gas in TMRs for two case studies (I, II).

Secondly, the effect of hydrogen mole fraction in the sweeping gas on the aromatic and hydrogen productions is investigated for two case studies in Fig.13 (a)-(b). The aromatic and hydrogen yields for the parallel configuration are higher than the serial one (see Fig.13 (a)-(b)). The effect of increasing the membrane thickness on the aromatic yield is slight. If case study II ($\delta_1=30\mu\text{m}$, $\delta_2=50\mu\text{m}$, $\delta_3=70\mu\text{m}$) is applied, the required compressor pressures decrease drastically, while no considerable changes are observed in the aromatic and

hydrogen production rates (compare Fig.12 and 13). The same trend is observed for total hydrogen production in Fig.13 (b).

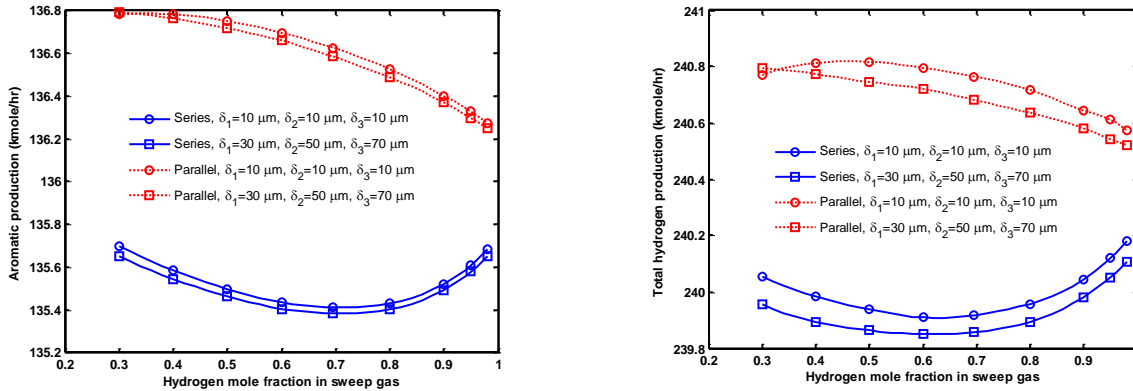


Figure.13 (a) Aromatic production (b) total hydrogen production versus the hydrogen mole fraction in the sweeping gas in TMRs for two case studies (I, II).

8. Conclusion

TMR with parallel and serial flows of the sweeping gas is modeled and compared with the plant data of CTR. Results show that TMR with the parallel configuration is superior to the serial one. Since three reactors in TMR operate independently for the parallel flow of the sweeping gas, parallel configuration can be advantageous if a defect happens for one of the reactors. Moreover, the sweeping gas acts as a secondary insulation. As a novel idea, the effect of hydrogen mole fraction in the sweeping gas and membrane thickness on the products yield and the required pressures of compressors are investigated for two case studies. Results show that by choosing thicker membranes (i.e., case study II) the required compressors' pressures decrease remarkably while the aromatic and hydrogen production rates do not change considerably. The optimization of the membrane thicknesses can be as a future work owing to obtaining better results in the case study II.

Appendix C. Nomenclature

Parameter	Dimension	Description
a	[-]	catalyst activity
A	[kmol h^{-1}]	moles of aromatic formed
A_c	[m^2]	cross-section of reactor
c_p	[$\text{kJ kmol}^{-1} \text{K}^{-1}$]	specific heat
c_t	[kmol m^{-3}]	molar concentration
E_d	[J mol^{-1}]	activation energy of catalyst
E_i	[kJ kmol^{-1}]	activation energy for i reaction
E_p	[kJ mol^{-1}]	activation energy of permeability
FBP	[$^{\circ}\text{C}$]	final boiling pint
F_t	[kmol h^{-1}]	total molar flow rate
h_f	[$\text{W m}^{-2} \text{K}^{-1}$]	Heat transfer coefficient
HC	[kmol h^{-1}]	Hydrocarbon
H_2	[kmol h^{-1}]	Hydrogen
ΔH	[kJ kmol^{-1}]	heat of reaction
IBP	[$^{\circ}\text{C}$]	initial boiling pint
k	[$\text{W m}^{-1} \text{s}^{-1}$]	thermal conductivity
k_{ci}	[m h^{-1}]	mass transfer coefficient for component i
k_{f1}	[$\text{kmol h}^{-1} \text{kgcat}^{-1} \text{MPa}^{-1}$]	forward rate constant for reaction (1)
k_{f2}	[$\text{kmol h}^{-1} \text{kgcat}^{-1} \text{MPa}^{-2}$]	forward rate constant for reaction (2)
k_{f3}	[$\text{kmol h}^{-1} \text{kgcat}^{-1}$]	forward rate constant for reactions (3)
k_{f4}	[$\text{kmol h}^{-1} \text{kgcat}^{-1}$]	forward rate constant for reactions (4)
K_{e1}	[MPa^3]	equilibrium constant
K_{e2}	[MPa^{-1}]	equilibrium constant
L	[m]	length of reactor
m	[-]	number if data sets used
m_c	[kg]	mass of catalyst

MR	$[-]$	membrane reactor
M_i	$[kg\ kmol^{-1}]$	molecular weight of component i
M_w	$[kg\ kmol^{-1}]$	average molecular weight of the feedstock
n	$[-]$	average carbon number for naphtha
N_A	$[kmol\ h^{-1}]$	molar flow rate of aromatic
N_i	$[kmol\ h^{-1}]$	molar flow rate of component i
$NPBR$	$[-]$	normal packed bed reactor
p	$[kmol\ h^{-1}]$	moles of paraffin formed
P_i	$[kPa]$	partial pressure of i component
P_t	$[kPa]$	total pressure
r_i	$[kmol\ kgcat^{-1}\ h^{-1}]$	rate of reaction for i reaction
R	$[kJ\ kmol^{-1}\ K^{-1}]$	gas constant
RON	$[-]$	research octane number
R_i	$[m]$	inner radius of palladium layer
R_o	$[m]$	outer radius of palladium layer
S_a	$[m^2\ kg^{-1}]$	specific surface area of catalyst pellet
t	$[h]$	Time
T	$[K]$	temperature of gas phase
TBP	$[^{\circ}C]$	true boiling point
T_s	$[K]$	temperature of solid phase
T_R	$[K]$	reference temperature
x	$[m]$	reactor length
y_i	$[-]$	mole fraction for i component in gas phase
y_{is}	$[-]$	mole fraction for i component on solid phase
V_c	$[cm^3\ kmol^{-1}]$	critical volume
Greek letters		
γ	$[-]$	shape factor of pellet
ϵ_b	$[-]$	void fraction of catalyst bed
μ	$[kg\ m^{-1}\ s^{-1}]$	viscosity of gas phase
ν_{ij}	$[-]$	Stoichiometric coefficient of component i in reaction j
ρ_b	$[kg\ m^{-3}]$	density of catalyst bed
ρ_g	$[kg\ m^{-3}]$	density of gas phase
Subscripts		
a	$[-]$	Aromatic
cal	$[-]$	Calculated
h	$[-]$	Hydrogen
lh	$[-]$	light hydrocarbon
n	$[-]$	Naphthene
out	$[-]$	Outlet
p	$[-]$	Paraffin

References

- [1] V.M. Benitez, C.R. Vera, M.C. Range, J.C. Yori, J.M. Grau, C.L. Pieck, Modification of Multimetallic Naphtha-Reforming Catalysts by Indium Addition, *Ind. Eng. Chem. Res.* 48, 671–676 (2009).
- [2] V.A. Mazzieri, C.L. Pieck, C.R. Vera, J.C. Yori, J.M. Grau, Effect of Ge content on the metal and acid properties of Pt-Re-Ge/Al₂O₃-Cl catalysts for naphtha reforming, *Appl. Catal. A*, 353, 93–100 (2009).
- [3] N. Viswanadham, R. Kamble, A. Sharma, M. Kumar, A.K. Saxena, Effect of Re on product yields and deactivation patterns of naphtha reforming catalyst, *J. Mol. Catal. A: Chem.* 282, 74–79 (2008).
- [4] M. Boutzeloit, V.M. Benitez, V.A. Mazzieri, C. Especel, F. Epron, C.R. Vera, C.L. Pieck, P. Marecot, Effect of the method of addition of Ge on the catalytic properties of Pt-Re/Al₂O₃ and Pt-Ir/Al₂O₃ naphtha reforming catalysts, *Catal. Commun.* 7, 627–632 (2006).

- [5] L.S. Carvalho, C.L. Pieck, M.C. Rangel, N.S. Figoli, C.R. Vera, J.M. Parera, Trimetallic naphtha reforming catalysts II. Properties of the acid function and influence of the order of addition of the metallic precursors on Pt-Re-Sn/-Al₂O₃-Cl, *Appl. Catal. A*, 269, 105–116 (2004).
- [6] J. Beltramini, A. Tanksale, Improved performance of naphtha reforming process by the use of metal zeolite composite catalysts, *Proceedings of 4th International FEZA Conference*, 2008.
- [7] X.H. Ren, M. Bertmer, S. Stapf, D.E. Demco, B. Blümich, C. Kern, A. Jess, Deactivation and regeneration of a naphtha reforming catalyst, *Appl. Catal. A*, 228, 39–52 (2002).
- [8] R.B. Smith, Kinetic analysis of naphtha reforming with platinum catalyst, *Chem. Eng. Prog.* 55(6), 76–80 (1959).
- [9] M.P. Ramage, K.P. Graziani, F.J. Krambeck, 6 Development of mobil's kinetic reforming model, *Chem. Eng. Sci.* 35, 41–48 (1980).
- [10] M.P. Ramage, K.R. Graziani, PH. Schipper, F.J. Krambeck, B.C. Choi, A review of Mobil's Industrial Process Modeling Philosophy, *Adv. Chem. Eng.* 13, 193-266 (1987).
- [11] H.G. Krane, A.B. Groh, B.L. Schuhnan, J.H. Sinfel, Reactions in Catalytic Reforming of Naphthas, Paper presented in fifth World Petroleum Congress (1960).
- [12] H. Weifeng, S. Hongye, H. Yongyou, C. Jian, Lumped kinetics model and its on-line application to commercial catalytic naphtha reforming process, *J. Chem. Ind. Eng.* 57(7) (2006).
- [13] W.S. Kmak, A Kinetic Simulation Model of the Powerformmg Process, *AIChE National Meeting* (1972).
- [14] R.S. Boyas, G.F. Froment, Fundamental Kinetic Modeling of Catalytic Reformer, *Ind. Eng. Chem. Res.* 48, 1107-1119 (2009).
- [15] M.Z. Stijepovic, A.V. Ostojic, I. Milenkovic, P. Linke, Development of a Kinetic Model for Catalytic Reforming of Naphtha and Parameter Estimation Using Industrial Plant Data, *Energy & Fuels* 23, 979-983 (2009).
- [16] G.B. Marin, G.F. Froment, J.J. Lerou, W. De Backer, Simulation of a Catalytic Naphtha Reforming Unit, *W. Eur. Fed. Chem. Eng.* 2 (27), 1–7 (1983).
- [17] D. Iranshahi, M.R. Rahimpour, A. Asgari, A novel dynamic radial-flow, spherical-bed reactor concept for naphtha reforming in the presence of catalyst deactivation, *Int. J. Hydrogen Energy* 35, 6261-6275 (2010).
- [18] M.R. Rahimpour, Enhancement of hydrogen production in a novel fluidized-bed membrane reactor for naphtha reforming, *Int. J. Hydrogen Energy* 34, 2235–2251 (2009).
- [19] I.M. Kolesnikov, V.I. Zuber, N.A. Svarovskaya, S.I. Kolesnikov, Reforming of naphtha cut in a fluidized bed of catalysis, *Chem. Technol. Fuels Oils*, Vol. 44, No. 3, (2008).
- [20] L.K. Min, G.H. Yan, P.S. Wei, A study on naphtha catalytic reforming reactor simulation and analysis, *Journal of Zhejiang University Science*, 2004.
- [21] M.R. Rahimpour, D. Iranshahi, A.M. Bahmanpour, Dynamic optimization of a multi-stage spherical, radial flow reactor for the naphtha reforming process in the presence of catalyst deactivation using differential evolution (DE) method, *Int. j. Hydrogen Energy* 35, 7498 -7511 (2010).
- [22] H. Weifeng, S. Hongye, M. Shengjing, C. Jian, Multiobjective Optimization of the Industrial Naphtha Catalytic Reforming Process, *Chin. J. Chem. Eng.* 15(1), 75-80 (2007).
- [23] H. Weifeng, S. Hongye, U. Yongyou, C. Jian, Modeling, Simulation and Optimization of a Whole Industrial Catalytic Naphtha Reforming Process on Aspen Plus Platform, *Chin. J. Chem. Eng.* 14(5), 584-591 (2006).
- [24] J. Li, Y. Tan, L. Liao, Modeling and Optimization of a Semi-regenerative Catalytic Naphtha Reformer, *Proceedings of the 2005 IEEE Conference on Control Applications*.
- [25] U.M. Taskar, Modeling and optimization of a catalytic naphtha reformer, Doctor of philosophy thesis, 1996.

- [26] T. Lid, S. Skogestad, Data reconciliation and optimal operation of a catalytic naphtha reformer, *J. Process Control* 18, 320–331 (2008).
- [27] H.F. Rase, *Chemical Reactor Design for Process Plants*, vol. 2, John Wiley & Sons, Inc., 1977.
- [28] A. Khosravanipour Mostafazadeh, M.R. Rahimpour, A membrane catalytic bed concept for naphtha reforming in the presence of catalyst deactivation, *Chem. Eng. Process.* 48, 683–694 (2009).
- [29] H.S. Fogler, *Elements of Chemical Reaction Engineering*, second ed., Prentice-Hall Englewood Cliffs NJ, 1992.
- [30] M.R. Rahimpour, S. Esmaili, G.N.A. Bagheri, Kinetic and deactivation model for industrial catalytic naphtha reforming, *Iran. J. Sci. Technol. Trans B Tech* 27, 279–90 (2003).
- [31] Operating Data of Catalytic Reformer Unit, Domestic Refinery, 2005.
- [32] R.G. Rice, D. Do, *Applied mathematics and modeling for chemical engineers*, John Wiley & Sons, New York, 1995.
- [33] R.H. Perry, D.W. Green, J.O. Maloney, *Perry's chemical engineers' handbook*, seventh ed., McGraw-Hill, 1997.
- [34] D.T. Jr, H. Kramers, Mass transfer from spheres in various regular packing to a flowing fluid, *Chem. Eng. Sci.* 8, 271 (1958).
- [35] C.R. Wilke, Estimation of liquid diffusion coefficients, *Chem.Eng.Prog.* 45(3), 218–224 (1949).
- [36] R.C. Reid, T.K. Sherwood, J. Prausnitz, *The Properties of Gases and Liquids*, third ed., McGraw-Hill, New York, 1977.
- [37] J.M. Smith, *Chemical engineering kinetics*, McGraw-Hill, New York, 1980.

*Corresponding author. (D. Iranshahi), Tel.: +98 21 64543196; fax: +98 21 6413969,
E-mail address: iranshahi@aut.ac.ir*

Appendix A. Orthogonal Collocation method

Jacobi Polynomials

The Jacobi function, $J_N^{(\alpha,\beta)}(x)$, is a polynomial of degree N that is, orthogonal with respect to the weighting function $x^\beta(1-x)^\alpha$. The Jacobi polynomial of degree N has the power series as follow:

$$J_N^{(\alpha,\beta)}(x) = \sum_{i=0}^N (-1)^{N-i} \gamma_{N,i} x^i \quad (\text{A-1})$$

The domain of x is in the range $[0, 1]$.

The evaluation of coefficients is done by using the following recurrence formula

$$\frac{\gamma_{N,i}}{\gamma_{N,i-1}} = \frac{N-i+1}{i} \cdot \frac{N+i+\alpha+\beta}{i+\beta} \quad (\text{A-2})$$

Starting with

$$\gamma_{N,0} = 1 \quad (\text{A-3})$$

$\gamma_{N,i}$ are constant coefficients, and α and β are parameters characterizing the polynomials.

Lagrange Interpolation Polynomials

For a given set of data points $(x_1, y_1), (x_2, y_2), \dots, (x_N, y_N)$ and (x_{N+1}, y_{N+1}) an interpolation formula passing through all $(N+1)$ points is an N^{th} degree polynomial. A suitable interpolation polynomial for the orthogonal collocation method is Lagrange interpolation polynomial, which passes through interior collocation points, roots of Jacobi polynomials, and it is expressed as

$$y_N(x) = \sum_{j=1}^{N+1} y_j l_j(x) \quad (\text{A-4})$$

where y_N is the N^{th} degree polynomial, y_i is the value of y at the point x_i , and $l_i(x)$ is defined as

$$l_i(x) = \prod_{\substack{j=1 \\ j \neq i}}^{N+1} \frac{(x - x_j)}{(x_i - x_j)} \quad (\text{A-5})$$

Furthermore,

$$l_i(x_j) = \begin{cases} 0 & i \neq j \\ 1 & i = j \end{cases} \quad (\text{A-6})$$

The first and second derivative at the interpolation points are:

$$\frac{dy_N(x_i)}{dx} = \sum_{j=1}^{N+1} \frac{dl_j(x_i)}{dx} y_j \quad (\text{A-7})$$

$$\frac{d^2 y_N(x_i)}{dx^2} = \sum_{j=1}^{N+1} \frac{d^2 l_j(x_i)}{dx^2} y_j \quad (\text{A-8})$$

For $i = 1, 2, \dots, N, N+1$.

The first derivative vector, composed of $(N+1)$ first derivatives at the $(N+1)$ interpolation points is:

$$y_N' = \left[\frac{dy_N(x_1)}{dx}, \frac{dy_N(x_2)}{dx}, \dots, \frac{dy_N(x_N)}{dx}, \frac{dy_N(x_{N+1})}{dx} \right]^T \quad (\text{A-9})$$

Similarly, the second derivative vector is defined as

$$y_N'' = \left[\frac{d^2 y_N(x_1)}{dx^2}, \frac{d^2 y_N(x_2)}{dx^2}, \dots, \frac{d^2 y_N(x_N)}{dx^2}, \frac{d^2 y_N(x_{N+1})}{dx^2} \right]^T \quad (\text{A-10})$$

The function vector is defined as values of y at $(N+1)$ collocation points as

$$y = [y_1, y_2, y_3, \dots, y_N, y_{N+1}]^T \quad (\text{A-11})$$

By means of these definitions of vectors y and derivative vectors, the first and second derivative vectors can be written in terms of the function vector y using matrix notation

$$y' = A \cdot y \quad (\text{A-12})$$

$$y'' = B \cdot y$$

Where the matrices A and B are defined as

$$A = \left\{ a_{ij} = \frac{dl_j(x_i)}{dx}; i, j = 1, 2, \dots, N, N+1 \right\} \quad (\text{A-13})$$

$$B = \left\{ b_{ij} = \frac{d^2 l_j(x_i)}{dx^2}; i, j = 1, 2, \dots, N, N+1 \right\} \quad (\text{A-14})$$

The matrices A and B are $(N+1, N+1)$ square matrices. Once the $(N+1)$ interpolation points are chosen, then all the Lagrangian building blocks, $l_i(x_i)$, are completely known, and thus the matrices A and B are also known [32].

Appendix B. Auxiliary Correlations

B.1 Gas phase viscosity

Viscosity of reactants and products is obtained from the following formula:

$$\mu = \frac{C_1 T^{C_2}}{1 + \frac{C_3}{T} + \frac{C_4}{T^2}} \quad (\text{B-1})$$

where μ is the viscosity in $Pa \cdot s$ and T is the temperature in K . Viscosities are at 1atm [33].

The constants of equation B-1 are presented in Table B.1.

Table B.1 Constant of Eq (B-1) for reactant and product.

Component	C1	C2	C3	C4
CnH2n+2	4.1306×10-8	0.9074	78.2449	0
CnH2n-6	3.6249×10-7	0.6063	208.5202	0
CnH2n	3.6744×10-7	0.5868	235.1696	0
H2	1.797×10-7	0.6850	-0.59	140
L.E	4.9054×10-8	0.90125	0	0

B.2. Gas phase Heat capacity

Heat Capacity of reactants and products at Constant Pressure is obtained from the following formula:

$$C_p = C_1 + C_2 \left[\frac{\frac{C_3}{T}}{\sinh\left(\frac{C_3}{T}\right)} \right]^2 + C_4 \left[\frac{\frac{C_5}{T}}{\cosh\left(\frac{C_5}{T}\right)} \right]^2 \quad (\text{B-2})$$

where c_p is in $J/(kmol K)$ and T is in K [33].

To complete the simulation, extra correlations should be added to the model. In the case of heterogeneous model, because of transfer phenomena, the correlations for estimation of heat and mass transfer between two phases should be considered. It is because of the concentration and heat gradient between bulk of the gas phase and the film of gas on the catalyst surface, which caused by the resistance of the film layer. The constants of equation B-2 are presented in Table B.2.

Table B.2 Constant of Eq (B-2) for reactant and product.

Component	C1×10-5	C2×10-5	C3×10-3	C4×10-5	C5
CnH2n+2	1.3781	4.4988	1.6369	3.053	746.85
CnH2n-6	1.166	4.6381	1.672	3.2894	781.46
CnH2n	0.8102	3.4545	1.5531	2.459	700.922
L.E	0.5192	1.9245	1.6265	1.168	723.6

B.3. Mass transfer correlations

To flow through a packed bed, the correlation is given by the following equation [34]:

$$\frac{k_{ci} d_p}{D_{im}} \frac{\varepsilon}{1-\varepsilon} \frac{1}{\gamma} = \left(\frac{u}{\mu(1-\varepsilon)\gamma} \right)^{1/2} \left(\frac{\mu}{\rho D_{im}} \right) \quad (\text{B-4})$$

where d_p is particle diameter (m), ε_b is void fraction of packed bed, is shape factor of pellet, u is superficial velocity through packed bed (m/s), is viscosity of gas fluid phase (kg/m s) and is fluid density (kg/m³).

Diffusivity of component i in the gas mixture is given by [35].

$$D_{im} = \frac{(1-y_i)}{\sum (y_i/D_{ij})} \quad (\text{B-5})$$

The binary diffusivities are calculated using the Fuller–Schetter–Giddins equation which is reported by Reid *et al.* [36]. In the following Fuller–Schetter–Giddins correlation, v_{ci} , M_i are the critical volume and molecular weight of component i which are reported in.

$$D_{ij} = \frac{10^{-7} T^{3/2} (1/M_i + 1/M_j)^{1/2}}{P_i (v_{ci}^{3/2} + v_{cj}^{3/2})^2} \quad (\text{B-6})$$

B.4. Heat transfer correlation

The heat transfer coefficient between the gas phase and solid phase is obtained by the following correlation [37]:

$$\frac{h_f}{c_p \rho \mu} \left(\frac{c_p \mu}{K} \right)^{2/3} = \frac{0.458}{\varepsilon_b} \left(\frac{\rho u d_p}{\mu} \right)^{-0.407} \quad (\text{B-7})$$

where in the above equation, u is superficial velocity of gas and the other parameters are those of bulk gas phase, d_p is the equivalent catalyst diameter, K is thermal conductivity of gas, ρ , μ are density and viscosity of gas, respectively and ε is void fraction of catalyst bed. Molecular weights and critical volumes of the components and other specifications of feed at inlet conditions are presented in Table B.3.

Table B.3 Molecular weights and critical volumes of the components and other specifications of feed at inlet conditions.

Parameter	Value	Dimension	Parameter	Value	Dimension
M_{wm}	21.8	g/mol	v_{ca}	0.375	m ³ /kmol
ρ_g	12.37	kg/m ³	v_{ch}	0.064	m ³ /kmol
c_{pg}	88.3	kJ/kmol k	$v_{cl.e}$	0.124	m ³ /kmol
μ	2.87×10^{-2}	cp	M_{wn}	113.9	g/mol
K	0.181	w/m k	M_{wp}	115.9	g/mol
v_{cp}	0.486	m ³ /kmol	M_{wa}	107.9	g/mol
v_{cn}	0.460	m ³ /kmol			